Cell, Vol. 112, 193–205, January 24, 2003, Copyright ©2003 by Cell Press

X-Ray Structures of Myc-Max and Mad-Max Recognizing DNA: Molecular Bases of Regulation by Proto-Oncogenic Transcription Factors

Satish K. Nair[2] and Stephen K. Burley[1,*]
Laboratories of Molecular Biophysics
Howard Hughes Medical Institute
The Rockefeller University
1230 York Avenue
New York, New York 10021

Summary

X-ray structures of the basic/helix-loop-helix/leucine zipper (bHLHZ) domains of Myc-Max and Mad-Max heterodimers bound to their common DNA target (Enhancer or E box hexanucleotide, 5′-CACGTG-3′) have been determined at 1.9 Å and 2.0 Å resolution, respectively. E box recognition by these two structurally similar transcription factor pairs determines whether a cell will divide and proliferate (Myc-Max) or differentiate and become quiescent (Mad-Max). Deregulation of Myc has been implicated in the development of many human cancers, including Burkitt's lymphoma, neuroblastomas, and small cell lung cancers. Both quasi-symmetric heterodimers resemble the symmetric Max homodimer, albeit with marked structural differences in the coiled-coil leucine zipper regions that explain preferential homo- and heteromeric dimerization of these three evolutionarily related DNA-binding proteins. The Myc-Max heterodimer, but not its Mad-Max counterpart, dimerizes to form a bivalent heterotetramer, which explains how Myc can upregulate expression of genes with promoters bearing widely separated E boxes.

Introduction

Since the identification of the *myc* genes as transforming agents within chicken retroviruses (Sheiness et al., 1978), compelling evidence has accumulated for their role in tumor formation both in experimental systems and in human malignancies (Cole and McMahon, 1999; Dang et al., 1999; Eilers, 1999; Liao and Dickson, 2000; Nesbit et al., 1999). Oncogenic activity of Myc protein is a direct result of deregulated expression and does not require mutations within the open reading frame. For example, in Burkitt's lymphoma the coding region for the cellular Myc (c-Myc) gene product is translocated to heavy or light chain genes of immunoglobulin loci, leading to deregulated patterns of Myc protein expression (Dalla-Favera et al., 1982; Taub et al., 1982). Related *myc* family genes, such as n-*myc* (neuroblastomas) and l-*myc* (small lung cancer), are also amplified and/or deregulated in malignancies (Kohl et al., 1983; Nau et al., 1985; Schwab et al., 1984). Finally, it is thought that *myc* genes are among the most frequently affected genes in human tumors (Nesbit et al., 1999).

The full-length Myc gene product is a *trans*-acting, DNA-binding regulator of transcription (Prendergast et al., 1991). All Myc isoforms contain two independently functioning polypeptide chain regions: N-terminal transactivating residues and a C-terminal basic-helix-loop-helix-leucine zipper (bHLHZ) segment (Figure 1A). The bHLHZ domain specifies dimerization through the helix-loop-helix-leucine zipper (HLHZ) region and DNA recognition via interactions between the basic (b) region and the major groove. Myc cannot form homodimers in vivo, at least at physiologic concentration, and does not support sequence-specific DNA binding in isolation.

A more complete understanding of Myc biology emerged following the discovery of a closely related bHLHZ protein, Max, which lacks an activation segment and serves as an obligate, physiological *hetero*dimerization partner for c-Myc (Blackwood and Eisenman, 1991; Prendergast et al., 1991). Myc function in transcriptional activation, cellular transformation, and apoptosis requires heterodimerization of the Myc and Max bHLHZ regions prior to sequence-specific DNA binding. Myc-Max heterodimers recognize a core hexanucleotide element (5′-CACGTG-3′), termed the Enhancer box or E box (Blackwood and Eisenman, 1991; Prendergast et al., 1991), and activate transcription at promoters containing such E boxes (Benvenisty et al., 1992; Eilers et al., 1991). Unlike Myc, Max can homodimerize and bind E boxes. At present, the precise biological role(s) of the Max homodimer remain unknown, but there are suggestions that Max can function as a transcriptional repressor (Kretzner et al., 1992). Sequence analyses of putative Myc target genes and the results of in vitro binding assays suggest that nucleotides flanking the E box element confer binding preferences for Myc-Max heterodimers versus Max homodimers (Grandori and Eisenman, 1997; Grandori et al., 1996).

The bHLHZ region of Myc has also been implicated in interactions with various cellular factors, including Nmi (Bao and Zervos, 1996), AP-2 (Gaubatz et al., 1995), Brca1 (Wang et al., 1998), and Miz-1 (Peukert et al., 1997). Interaction of Myc-Max heterodimer with Miz-1 has been validated but other reported interactions are not well characterized. Each of these molecules regulate gene expression, and their interactions with bHLHZ transcription factors appear to be limited to associations with the bHLHZ region of Myc (Sakamuro and Prendergast, 1999). Such higher order interactions document a role for Myc in targeting factors to particular promoter regions and suggest that the bHLHZ portions of the Myc-Max heterodimer play an architectural role in stabilizing nucleoprotein assemblies, such as enchanceosomes (Carey, 1998; Merika and Thanos, 2001).

Soon after the discovery of Max, a second class of bHLHZ proteins, including Mad1 (Ayer et al., 1993) and Mxi1 (Zervos et al., 1993) were independently shown to heterodimerize with Max and recognize E boxes. Subse-

*Correspondence: stephen_burley@stromix.com
[1]Present Address: Structural GenomiX, Inc., 10505 Roselle Street, San Diego, California 92121.
[2]Present Address: Department of Biochemistry and Center for Biophysics and Computational Biology, University of Illinois at Urbana-Champaign, 600 South Mathews Avenue, Urbana, Illinois 61801.

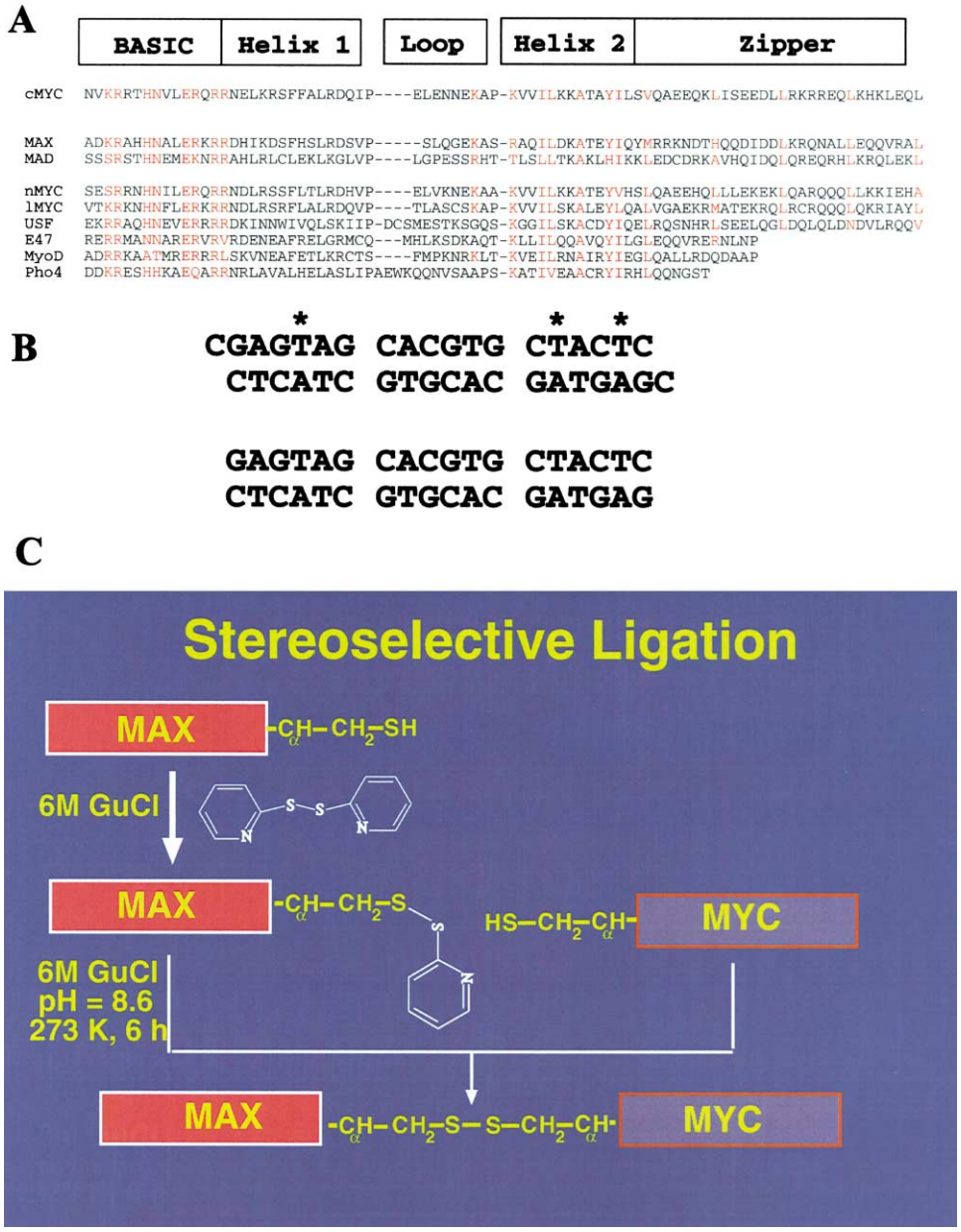

Figure 1. Myc, Max, and Mad Primary Sequences, Crystallization Oligonucleotides, and Semisynthetic Scheme for Chemoselective Ligation

(A) Partial sequence alignment of the DNA binding domains of human cMyc protein with the bHLHZ proteins Max, Mad, nMyc, lMyc, USF, E47, MyoD, and Pho4. Secondary structure assignments are based on X-ray crystal structures (where available) and conserved residues are highlighted in red.

(B) Sequence of the duplex oligonucleotides used in crystallization with Myc-Max (upper) and Mad-Max (lower). Positions of 5-iodo-dUra substitutions for heavy atom derivatives are denoted with an asterisk (*).

(C) Semisynthetic scheme used for the production of chemoselectively ligated Myc-Max and Mad-Max heterodimers (Experimental Procedures).

quent identification and characterization of Mad1 paralogs demonstrated similar functions (Hurlin et al., 1994). High levels of *mad* mRNA and Mad protein are found in growth arrested, differentiated cells in which c-Myc is not expressed. Moreover, Mad protein inhibits cell growth and interferes with the transforming function of Myc, demonstrating that Mad-Max is a transcriptional repressor (Hurlin et al., 1994; Larsson et al., 1997, 1994; McArthur et al., 1998).

Further advances in our understanding of transcriptional repression by the Mad-Max heterodimer emerged after identification of interactions between Mad and mSin3, a corepressor (Ayer et al., 1995; Schreiber-Agus et al., 1995). Mad-Max heterodimers recruit mSin3 corepressors to promoter DNA, which leads to recruitment of histone deacetylases, condensation of chromatin structure, and reduced transcription levels (Hassig et al., 1997; Laherty et al., 1997). Conversely, the ATM-related c-Myc binding protein TRRAP interacts with Myc-Max heterodimers to mediate recruitment of his-

tone acetyltransferases and upregulation of gene expression (Cole and McMahon, 1999; McMahon et al., 2000; Saleh et al., 1998). Thus, competition between Myc-Max and Mad-Max heterodimers for common DNA targets appears to control cell fate, determining the choice between proliferation/transformation and differentiation/quiescence.

The X-ray structure of the Max homodimer bound to an E box, derived from the Adenovirus major late promoter, established the structural bases for DNA recognition by bHLHZ proteins (Ferre-D'Amare et al., 1993). Our cocrystal structure revealed that Max dimerizes to form an asymmetric, parallel left-handed four-helix bundle composed of two pairs of right-handed α helices (b-H1 and H2-Z). The basic region projects from the N-terminal face of the four-helix bundle and interacts with DNA via sequence-specifying contacts with the major groove edges of base pairs comprising the E box. C-terminal extensions of two α helices form a left-handed coiled-coil or leucine zipper. More recently published X-ray studies of a related protein involved in regulation of cholesterol levels in humans (SREBP1; Parraga et al., 1998) documented that the structure of the bHLHZ dimer is essentially identical among bHLHZ family members.

In this paper, we report cocrystal structures of chemoselectively ligated c-Myc-Max (hereafter Myc-Max) and Mad1-Max (hereafter Mad-Max) heterodimers bound to duplex oligonucleotides containing E boxes. Although both heterodimers resemble the Max homodimer (Brownlie et al., 1997; Ferre-D'Amare et al., 1993), marked differences exist within the leucine zipper regions. Site-directed mutagenesis combined with protein-protein interaction assays documented that these structural differences account for preferential heterodimer formation among Myc, Mad, and Max. Within our Myc-Max cocrystals, two heterodimers associate tightly to form a bivalent heterotetramer that explains previously published biochemical observations. The biological significance of Myc-Max oligomerization is discussed in the context of our cocrystal structures.

Results and Discussion

Formation of Covalent Myc-Max and Mad-Max Heterodimers Via Chemoselective Ligation

Structural and biophysical characterization of Myc-Max and Mad-Max heterodimers was complicated by Max protein homodimerization at high concentrations (i.e., 0.1–1 mM). To overcome this problem and increase the likelihood of successful crystallization trials, a semisynthetic strategy (Baca et al., 1995) was used to produce pure preparations of chemoselectively ligated Myc-Max and Mad-Max heterodimers. Minimal bHLHZ domains of c-Myc (Watson et al., 1983; Watt et al., 1983), Max (Blackwood and Eisenman, 1991), and Mad1 (Ayer et al., 1993), each bearing a Gly-Gly linker followed by a Cys at their C-termini (Figure 1A), were expressed in *E. coli*. The sulfhydryl group in Max-Gly-Gly-Cys was derivatized with 2,2′-dipyridyl disulfide, and the resulting Max-pyridylsulfenyl cysteine adduct was purified from unmodified protein by reverse phase HPLC. (This step adds a leaving group to the Cys residue at the C terminus of Max, which enables chemoselective ligation with C-terminal Cys forms of either Myc or Mad.) Incubation of Myc-Gly-Gly-Cys (or Mad-Gly-Gly-Cys) with the Max-pyridylsulfenyl-cysteine adduct under denaturing conditions lead to thiolysis of the (2-pyridylsulfenyl)-cysteine by the C-terminal Cys of Myc (or Mad), resulting in highly efficient formation of directed disulfide-linked heterodimers (Figure 1C). Each heterodimer was then refolded and further purified using standard methods (Experimental Procedures). Analytical reverse phase HPLC and electrospray ionization mass spectrometry (ESI-MS) were used to identify all reaction intermediates and confirm that we had obtained the desired heterodimeric products. Electrophoretic mobility shift assays (EMSA) with E box containing oligonucleotides demonstrated high affinity, specific DNA-binding activity for the chemoselectively ligated Myc-Max and Mad-Max heterodimers, which compared favorably to the DNA-binding properties of native, unligated Max, and disulfide-linked Max homodimers (data not shown).

Crystallization and Structure Determination

Reconstituted heterodimers were mixed with a stoichiometric excess of oligonucleotide, and the desired protein-DNA complexes were purified by size exclusion chromatography and subject to crystallization trials. Twenty-three different C- and/or N-terminal truncations of the Myc and Max bHLHZ domains and over two hundred duplex oligonucleotides were screened before diffraction quality cocrystals were obtained (Experimental Procedures). The proteins used for structure determination encompass human Myc residues 353–434 (hereafter Myc), Max residues 22–103 (hereafter Max), and Mad residues 55–136 (hereafter Mad).

Experimental phases for the Myc-Max heterodimer cocrystal structure were determined at 2.8 Å resolution using three halogenated-DNA heavy atom derivatives. Our previously determined Max cocrystal structure (Ferre-D'Amare et al., 1993) was positioned in the experimental electron density using a brute force phased translation search (B. Strokopytov and S. Almo, personal communication) and the quality of the experimental phases was improved by non-crystallographic symmetry averaging and phase extension to 1.9 Å resolution (Experimental Procedures). The cocrystal structure of the Mad-Max heterodimer was determined via molecular replacement, using the structure of the Myc-Max heterodimer as a search model, and refined to 2.0 Å resolution. A summary of the crystallographic analyses is provided in Table 1.

Structure of the Myc-Max and Mad-Max bHLHZ Heterodimers

Three-dimensional structures of the Myc-Max and Mad-Max heterodimers are illustrated in Figure 2. These structures recapitulate the disposition of secondary structural elements observed in our cocrystal structures of the Max and SREBP1 homodimers (Ferre-D'Amare et al., 1993; Parraga et al., 1998). Each half of the heterodimer consists of two long α helices separated by a short random coil loop region (L). The N-terminal α helix represents a continuous secondary structural element encompassing both the basic region (b) and α helix

Table 1. Statistics of Crystallographic Analysis

Myc-Max Data set	Beamline	Wavelength (Å)	Resolution (Å)	Reflections (%) (total/unique)	Completeness (total/outer shell)	R_{sym} (%)	# Sites (total/unique)	Phasing power Iso	Phasing power Ano
Native 1	NSLS-X9A	0.92	2.3	134,509/25,186	96.5/90.6	5.2	–	–	–
Iodo 1	NSLS-X9A	1.54	2.5	57,481/18,071	93.1/91.1	5.6	8/8	2.4	1.9
Iodo 2	NSLS-X9A	1.54	2.5	103,200/17,699	90.5/88.4	6.4	8/4	1.0	0.7
Iodo 3	NSLS-X9A	1.54	2.7	61,374/11,919	76.4/58.7	5.8	4/0	1.1	–
Native 2	APS-19ID	0.91	1.8	276,421/49,228	95.9/90.9	5.3	–	–	–

Refinement against Native 2	
Resolution (Å)	20–1.8
Number of atoms	
Proteins	2759
DNA	1540
Solvent	581
R_{cryst}/R_{free} (%)	21.9/26.3
RMSD bond length (Å)	0.005
RMSD bond angles (°)	0.95

Mad-Max Data set	Beamline	Wavelength (Å)	Resolution (Å)	Reflections (%) (tot./unique)	Completeness (tot./outer shell)	R_{sym} (%)
Native 1	NSLS-X25	0.92	2.0	214,612/35,483	88.8/59.9	5.2

Refinement	
Resolution (Å)	20–2.0
Number of atoms	
Proteins	2509
DNA	1467
Solvent	251
R_{cryst}/R_{free} (%)	26.4/32.4
RMSD bond length (Å)	0.006
RMSD bond angles (°)	0.94

$R_{sym} = \Sigma|I - \langle I\rangle|\Sigma I$, where I is the observed intensity and $\langle I\rangle$ is the average obtained from multiple observations of symmetry related reflections.
Phasing power = rmsd (F_H/E), where F_H = heavy atom structure factor amplitude and E = residual lack of closure.
$R_{cryst} = \Sigma||F_{observed}| - |F_{calculated}||/\Sigma|F_{observed}|$, $R_{free} = R_{cryst}$ calculated using 10% random data omitted from the refinement.

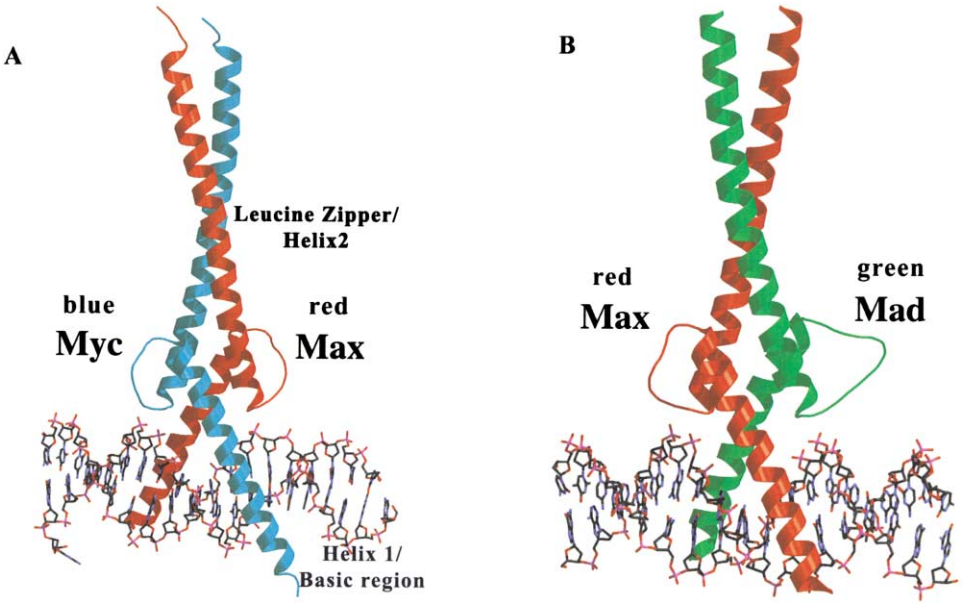

Figure 2. Structures of Myc-Max and Mad-Max Heterodimers Bound to DNA

Molscript (Kraulis, 1991)/Raster3D (Merritt and Murphy, 1994) drawing showing the overall topology of the Myc-Max/DNA (A) and Mad-Max (B) cocrystal structures. Color coding: Myc-cyan, Max-red, and Mad-green. Cocrystallization oligonucleotide is shown as an atomic stick figure. The helix, basic region, and zipper regions have been designated on the Myc-Max/DNA structure.

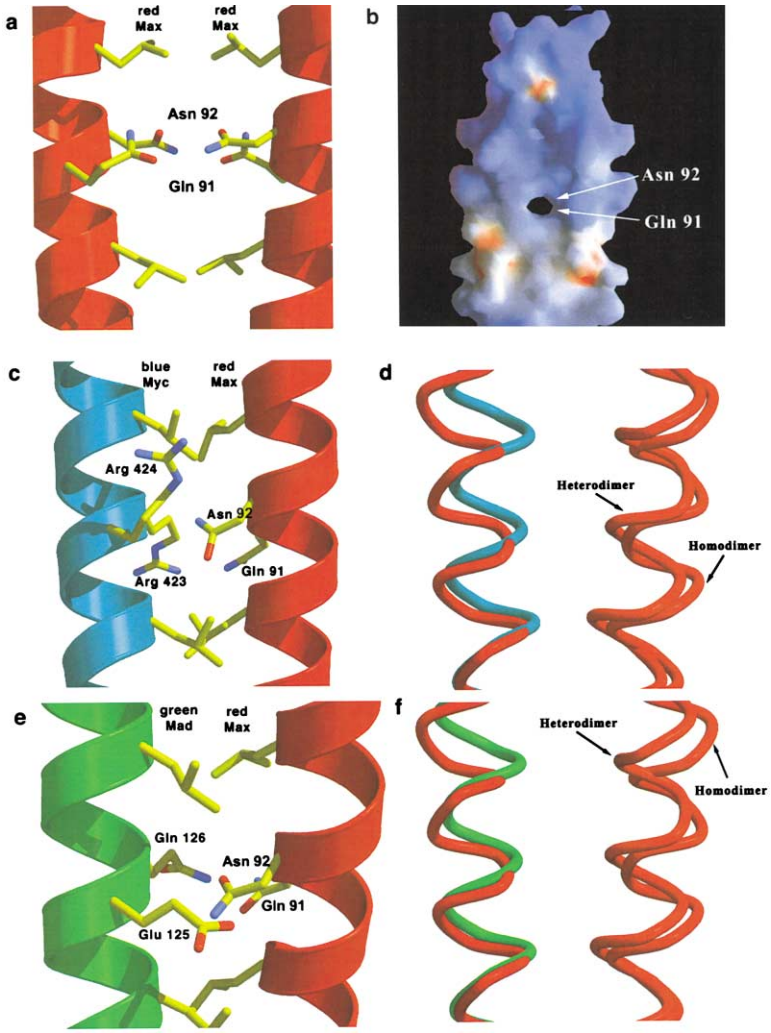

Figure 3. Comparison of Homo- and Heterodimeric bHLHZ Complexes

(A) Ribbon diagram of the Max homodimer (red), showing the C-terminal region of the leucine zipper. Residues comprising the Gln91-Asn92-Gln91*-Asn92* tetrad at the intermolecular interface are shown as atomic stick figures.

(B) GRASP (Nicholls et al., 1991) representation of the molecular surface of the Max homodimer showing bulging of the α helices with the resulting packing defect, viewed as in Figure 3A.

(C) Ribbon diagram of the Myc-Max heterodimer (Myc-blue; Max-red), viewed as in Figure 3A. Hydrogen bond pairs created by the disposition of Gln-Asn-Arg-Arg residues in the tetrad region yield a tighter dimer interface.

(D) Least squares superposition of the α carbon coordinates of the Max homodimer with the Myc-Max heterodimer (Myc-blue; Max-red) demonstrates that the leucine zipper regions of these crystal structures deviate significantly in the vicinity of the region of the Gln-Asn tetrad in the Max homodimer.

(E) Ribbon diagram of the Mad-Max heterodimer (Mad-green; Max-red), viewed as in Figure 3A. The Gln-Asn-Glu-Gln tetrad forms a tight dimer interface.

(F) Least squares superposition of the α carbon atomic coordinates of the Max homodimer with the Mad-Max heterodimer (Mad-green; Max-red), showing the same phenomenon as illustrated in Figure 3D.

H1. The C-terminal α helix is also comprised of two continuous α-helical segments, H2 and the leucine zipper (Z).

Two Leucine Zipper Residues Specify Heterodimerization with Max

The bHLHZ segments of Myc and Max, or Mad and Max, form quasisymmetric heterodimers that are stabilized by hydrophobic and polar interactions involving α helices H1, H2, and the leucine zipper region (Z). These extensive interfaces (buried solvent-accessible surface areas: Myc-Max = 3206 Å^2, Mad-Max = 2970 Å^2) are predominantly hydrophobic, with additional intermolecular contacts coming from hydrogen bonds along the periphery of the leucine zipper. Much of this coiled coil resembles GCN4 homodimer (Ellenberger et al., 1992; O'Shea et al., 1991), and consists of a heptad repeat (**abcdefg**) with hydrophobic residues at positions **a** and **d**. In our Max homodimer structure, however, a Gln91-Asn92-Gln91-Asn92 tetrad occurs near the C-terminal end of the zipper region, with Gln91 at position **g** of one heptad and Asn92 at position **a** of the following heptad (Figure 3A). This packing scheme alters the trajectories of the two α helices making up the coiled coil, which is manifested by flaring of the leucine zipper (Figure 3A) and creation of a packing defect within the interface (Figure 3B).

In marked contrast, the leucine zipper regions of the Myc-Max (Figures 3C and 3D) and Mad-Max (Figures 3E and 3F) heterodimers closely resemble the coiled coils found in GCN4 homodimers (Ellenberger et al., 1992; O'Shea et al., 1991). Least squares superpositions of the α carbon coordinates of the Max homodimer with each heterodimer demonstrate that the leucine zipper regions of the heterodimers only deviate significantly in the vicinity of the Max-Max Gln91-Asn92-Gln91*-Asn92* tetrad (* denotes dimeric partner; root-mean-square deviations or rmsds: Myc-Max versus Max-Max = 1.5 Å, Mad-Max versus Max-Max = 1.6 Å, Myc-Max versus Mad-Max = 1.6 Å). In the Myc polypeptide chain, two positively charged residues (Arg423-Arg424) occupy this position yielding an Arg423-Arg424-Gln91-Asn92 tetrad within the Myc-Max heterodimer (Figure 3C). The hydrogen bond pairs mediated by these polar residues yield a more intimate dimer interface and result in tighter intermolecular packing (Figure 3D). A similar situation pertains to the Mad-Max heterodimer, with Glu125 of Mad and Asn92 of Max forming a hydrogen bond (OE2-ND2 = 2.79 Å; Figures 3E and 3F).

Conclusive identification of dimer specificity determi-

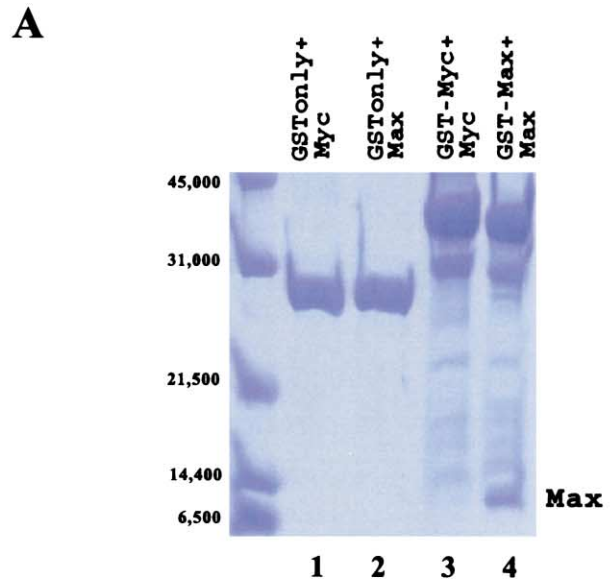

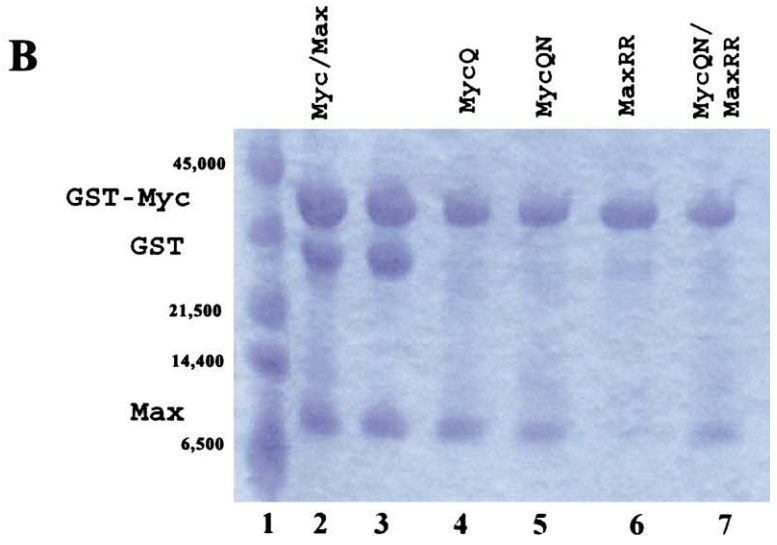

Figure 4. Homo- and Heterodimerization Assays with Myc and Max Tetrad Mutants

(A) Coomassie blue-stained SDS/PAGE gel of GST-affinity assays showing lack of binding of wild-type Myc or wild-type Max to GST alone (lanes 1 and 2), lack of binding of wild-type Myc to GST-Myc (lane 3) and binding of wild-type Max to GST-Max (lane 4).

(B) Coomassie blue-stained SDS/PAGE gel of GST-affinity assays shows binding of wild-type Max to wild-type Myc (lanes 2 and 3), Myc (Arg423→Gln) (lane 4), Myc (Arg423→Gln/Arg424→Asn) (lane 5) and binding of Max (Gln91→Arg/Asn92→Arg) to wild-type Myc (lane 6) and Myc (Arg423→Gln/Arg424→Asn) (lane 7).

nants within the Myc family was provided by a series of single and double-mutant variations of tetrad pairing that generate mutant homo- and heterodimers encompassing every possible exchange permutation between Myc and Max. Mutant proteins were purified to homogeneity and characterized by GST-mediated pull-down assays (Figure 4). As expected, wild-type Max interacts stably with both itself and with wild-type Myc, and replacement of Arg423 of Myc with Gln does not preclude heterodimerization with Max. Furthermore, the Myc double mutant (Arg423→Gln/Arg424→Asn), which recapitulates the tetrad observed in the Max homodimer, also interacts with wild-type Max. In contrast, a double-mutant form of Max (Gln91→Arg/Asn92→Arg) exhibited no detectable interaction with wild-type Myc. This finding can be explained by Coulomb repulsion of positively charged guanidium groups of the mutant Max (Gln91→Arg/Asn92→Arg) by the naturally occurring Arg423/Arg424 pair in wild-type Myc. As predicted, this mutant form of Max does form a stable heterodimer with the Myc mutant (Arg423→Gln/Arg424→Asn), because the hydrogen bonds observed in the wild-type Myc-Max heterodimer are restored by this set of double mutants, albeit in opposite orientation.

These results imply that homo- and heterodimerization specificity and avidity of Myc for Max are solely mediated by the identities of the amino acids at positions 91 and 92 (Max numbering). Not surprisingly, the charge-neutral Gln91-Asn92-Gln91*-Asn92* tetrad can support Max homodimerization, whereas the tetrad of positively

charged guanidium groups (Arg423-Arg424-Arg423*-Arg424*) disfavors Myc homodimerization. Myc-Max heterodimerization is favored over Max homodimerization by disposition of complementary polar residues at these positions within Myc and Max resulting in hydrogen bond pairing within the heterodimer interface.

It is remarkable that Mad-Max heterodimerization appears to be controlled by the identity of a single interfacial amino acid (Glu125). Model building studies with mutant forms of Mad suggest that the hetero- and homodimerization properties of Mad can be similarly manipulated by modifying Glu125 and Gln126 (data not shown). Mad residue Glu125 establishes a network of complementary hydrogen bond interactions at the tetrad interface that supports heterodimerization with Max. Glu125 OE2 engages ND2 of Max residue Asn92* (2.79 Å). In turn, OD1 of Asn92* hydrogen bonds to NE2 of Gln126 (3.29 Å), which, itself, hydrogen bonds to OE1 of Gln 91* (3.07 Å).

Structural Basis of E Box Recognition

In order to avoid the effects of twofold averaging of the oligonucleotide about the internal pseudo dyad imposed by the palindromic E box, we used a symmetric oligonucleotide for our cocrystallization experiments. In both of our heterodimer cocrystal structures, the DNA adopts a modified B form conformation, characterized by a narrowed major groove and a widened minor groove (Nekludov and Pabo, 1994). There is no evidence of DNA bending in contrast to a cocrystal structure of Max homodimer (Brownlie et al., 1997) and gel mobility and phasing analysis studies that were interpreted to show a bend of up to 80° toward the minor groove (Fisher et al., 1992).

The cocrystal structures of the Myc-Max and Mad-Max heterodimers bind to their respective DNA targets with each component of the heterodimer interacting with half of the 5′-CACGTG-3′ recognition site. Myc, Max, and Mad use essentially identical protein-DNA contacts for recognition of the E box to those detected in our Max homodimer structure (Ferre-D'Amare et al., 1993). Four sequence-specifying contacts are made between each basic region and selected DNA bases within the recognition sequence 5′-Cyt(1)-Ade(2)-Cyt(3)-Gua(4)-Thy(5)-Gua(6)-3′, including NE2 of His28 (Myc: His359; Mad: His61) and N7 of Gua(3′), where ' denotes opposite strand (see Figure 1), OE1 of Glu32 (Myc: Glu363; Mad: Glu65) with N4 of Cyt(3) and OE2 of Glu32 with N6 of Ade(2), and NH1 of Arg36 (Myc: Arg-367; Mad: Arg69) with N7 of Gua(1'). The contact made by Arg36 dictates the identity of the central 5′-CG-3′ dinucleotide and distinguishes bHLHZ proteins that bind class A E box elements from those that bind the non-canonical class B site (5′-CAGCTC-3′), such as AP4 (Dang et al., 1992). A single amino acid substitution (Arg36→Met) suffices to convert AP4 into a canonical class A E box binding protein (Dang et al., 1992).

Several additional contacts are observed between residues specific to Myc and the phosphate backbone: NZ of Lys355 forms hydrogen bonds with both phosphate oxygens of Gua(-4) (NZ-O1P = 3.6 Å: NZ-O2P = 3.3 Å), Arg356 hydrogen bonds with backbone phosphate oxygen of Thy(5) (NH1-O2P = 2.7 Å). In addition, two residues within the loop region of Myc make nonspecific hydrogen bond contacts: NZ of Lys371 with O1P of Ada(2) (3.2 Å) and NZ of Lys 392 with O1P of Ada(2) (2.9 Å). Combinatorial solid-phase peptide synthesis and DNA affinity studies by Winston and Gottesfeld have identified the role of loop residues of bHLH proteins in contributing to DNA-binding (Winston and Gottesfeld, 2000).

Site-directed mutagenesis and basic region swap experiments between Myc and Max have suggested that the Myc and Mad proteins are not functionally equivalent and have separable E box binding activities (O'Hagan et al., 2000). Specifically, mutation of Myc residue Arg357 supports a role for this residue in oncogenic potency. Within our crystal structure, Arg357 is faces away from the DNA and is not involved in direct interactions with the E box or flanking nucleotides. As suggested by the authors, it is conceivable that the observed effects of mutation at Arg357 at the Myc basic region may be mediated by inter- or intramolecular interactions with other proteins, but these suggestions have yet to be experimentally confirmed.

Crystal Structure Reveals a Bivalent Myc-Max Heterotetrameter

The two Myc-Max/DNA complexes constituting the asymmetric unit in our cocrystals are related by a noncrystallographic 2-fold rotation. The most remarkable feature of this intimate dimer of heterodimers is the head-to-tail assembly of the individual leucine zippers of each heterodimer, resulting in formation of an antiparallel four-helix bundle (Figure 5A). This four-helical bundle is topologically similar to helical bundles observed in members of the cytokine family and in leukemia inhibitory protein (Hill et al., 1993; Somers et al., 1997; Robinson et al., 1994).

Salt bridges and hydrogen bonds, burying nearly 1400 Å^2 of solvent-accessible surface area, mediate packing interactions between the two heterodimers (Figure 5B). Within this head to tail arrangement of leucine zippers, Max residue Lys77 from one heterodimer interacts with Glu432$^{\#}$ ($^{\#}$ denotes second heterodimer of bivalent tetramer) of Myc from the second heterodimer (NZ-OE2 = 2.6 Å) and is situated near the backbone carbonyl oxygens of Lys428$^{\#}$ and His429$^{\#}$. Myc residue Glu425$^{\#}$ is situated within a positively charged region within the tetramer interface comprising Max residues Lys77 (OE1-NZ = 4.1 Å) and His-81 (OE1-NE2 = 3.8 Å), which, in turn, faces toward the backbone carbonyls of Lys423$^{\#}$ and Glu425$^{\#}$. Myc residue Glu417$^{\#}$ makes polar contacts with Myc residues Arg-424 and Arg421 from the second heterodimer and Arg424 faces toward Max residue Asp84$^{\#}$.

Previously published in vivo and in vitro studies have shown that Myc-Max heterodimers can form higher order oligomers. Solution studies (Dang et al., 1989) by Dang and coworkers demonstrated that Myc-Max is capable of forming bivalent heterotetramers and that tetramerization depends on Myc leucine zipper region. Several lines of evidence suggest that the bivalent heterotetramer observed in our Myc-Max cocrystals exists under physiological conditions. First, solution experiments demonstrated that the Myc-Max heterodimer

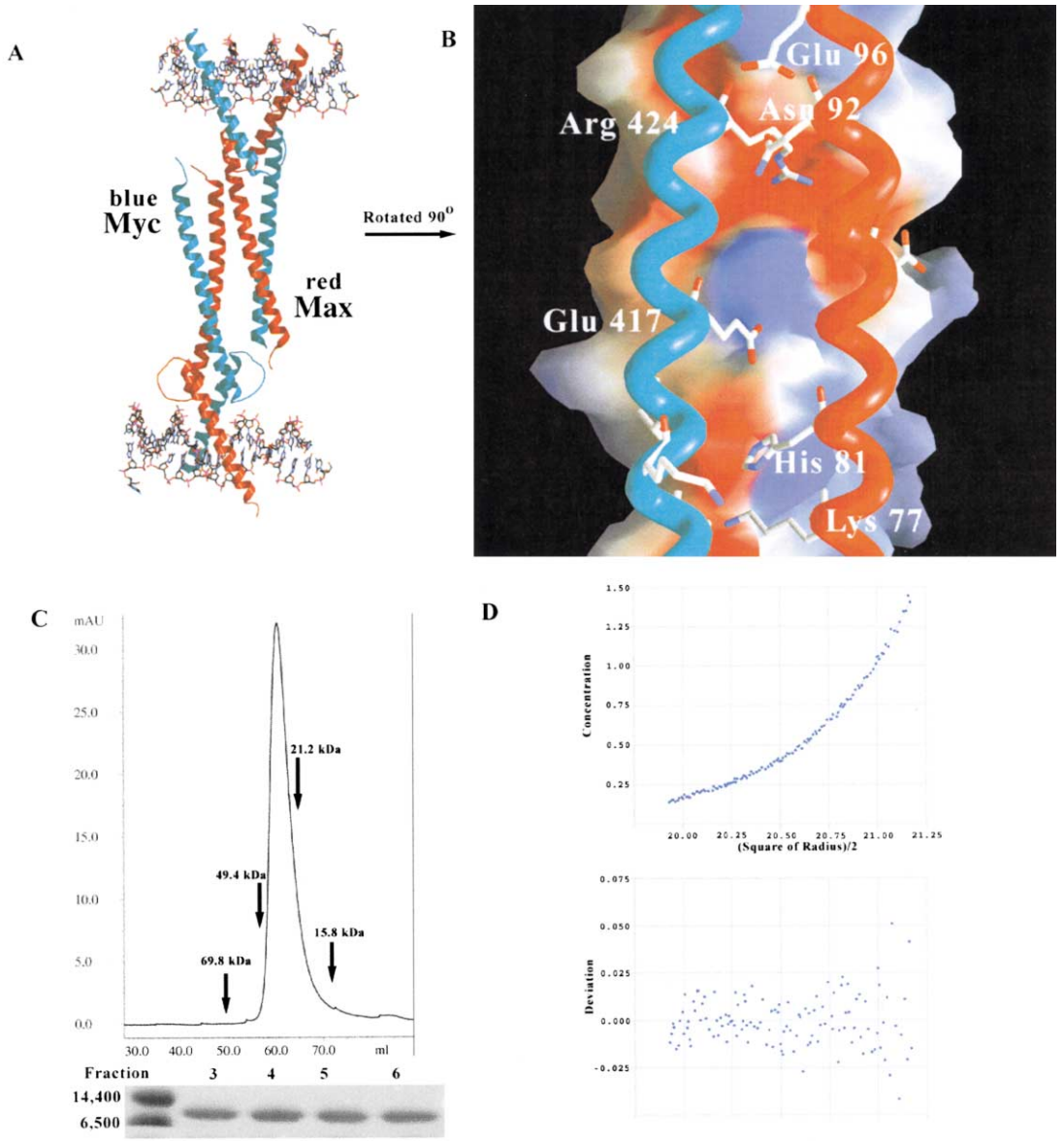

Figure 5. Bivalent Myc-Max Heterotetramer

(A) Ribbon diagrams of the bivalent Myc-Max heterotetramer observed in the Myc-Max/DNA cocrystals.

(B) GRASP (Nicholls et al., 1991) molecular surface rendition of one heterodimer with α carbon backbone representation (cyan and red) of the other. The view is orthogonal to the orientation in Figure 5A. Salt bridges and hydrogen bonds, burying nearly 1400 Å^2 of solvent-accessible surface area, mediate packing interactions between the two heterodimers. The polarity of many of the residues in Myc that comprise this interaction network is altered in Mad and this alteration in polarity of the residues that stabilize the interaction of the Myc-Max heterotetramer may explain the lack of tetramer formation by Mad-Max heterodimers.

(C) Size exclusion profile of the Myc-Max heterodimer. Approximately, 300 μM of the heterodimer was loaded onto a Superdex 75 column (Pharmacia) and representative fractions from the elution run are shown on a Coomassie blue-stained SDS/PAGE gel. Elution volumes for four calibration standards are noted on the chromatogram. Myc-Max elutes at a position corresponding to a relative molecular mass of approximately 40 kDa corresponding to the expected size of the Myc-Max heterotetramer observed in the crystals.

(D) Hydrodynamic characterization of the Myc-Max bivalent heterotetramer. Sedimentation equilibrium data were collected at 280 nm with a rotor speed of 20,000 rpm at a temperature of 20°C using a Beckman XL-A ultracentrifuge. The fit corresponds to a two-component model with a tethered Myc-Max dimer to Myc-Max tetramer association constants of 90 nM. The residuals of the fit are shown in the lower image. Data analysis utilized the NONLIN program (http://www.cauma.uthscsa.edu/software).

can form a tetramer at sub-μmolar concentrations (Figure 5C) and analytical ultracentrifugation studies revealed a tetramer-dimer equilibrium dissociation constant of 90 nM (Figure 5D). Published quantitative analyses of c-Myc copies per proliferating cells estimate 6,300 c-Myc molecules in MRC5 fibroblasts as determined by enzyme-linked immunosorbent assay (Moore et al., 1987) or 29,000 c-Myc molecules for IMR90 fibroblasts as determined by quantitative Western blotting (Rudolph et al., 1999). Assuming a homogenous distribu-

tion of c-Myc molecules within a spherical nucleus with a diameter of 5.0 μM, these estimates correspond to nuclear c-Myc concentrations of 152 nM (for MRC5 fibroblasts) or 764 nM (for IMR90 fibroblasts). Given that our measured dissociation constant of 90 nM is lower than either of the two estimates of physiological c-Myc levels, our data conclusively document that c-Myc-Max exists as a bivalent heterotetramer at physiologic concentrations. Second, solvent-accessible surface area burial on bivalent heterotetramer formation is 1375 Å^2, which is well in excess of the accepted upper limit of 600 Å^2 for adventitious lattice-packing contacts (Janin, 1997). Finally, electron microscopic studies with synthetic *myc* promoters containing multiple E-boxes separated by distances of 100–200 nucleotides demonstrated that the Myc-Max heterodimer can engage spatially disparate E box binding sites, presumably via higher order oligomerization (T. Haggerty, and C.V. Dang, personal communication).

The biological relevance of the bivalent heterotetramer observed in our Myc-Max cocrystals is borne out by a wealth of genetic and biochemical data. Work from a number of laboratories has shown that Myc-Max can recruit various cellular factors, most convincingly Miz-1 (Peukert et al., 1997) but also including Nmi (Bao and Zervos, 1996), AP-2 (Gaubatz et al., 1995), and Brca1 (Wang et al., 1998). Each of these higher order assemblies result from specific interactions with the bHLHZ region of Myc (Sakamuro and Prendergast, 1999). Given that all of these proteins are transcription factors, which are recruited to specific regions of the promoter, it seems reasonable to suggest that the bHLHZ regions of the Myc-Max heterodimer play an architectural role. Formation of the bivalent heterotetramer observed in our cocrystal structure would provide a substantial platform for assembly of additional protein factors.

Genetic characterization of the promoters of putative *myc* regulated genes has provided further evidence for a physiological role for Myc-Max heterotetramerization. Oligonucleotide microarray analysis has identified several Myc target genes that contain multiple E boxes within promoters, typically separated by at least 100 nucleotides (Coller et al., 2000; see also Grandori and Eisenman, 1997). Given the persistence length of DNA, this separation of Myc-Max binding sites is compatible with DNA looping stabilized by bivalent Myc-Max heterotetramers bound to two cognate sequences. Moreover, in vitro binding studies of Myc-Max heterodimers recognizing the lactate dehydrogenase gene, a natural high-affinity target containing two consensus E boxes (Shim et al., 1997), demonstrates that Myc-Max complexes can engage multiple cognate sites. Functional studies with adjacent E boxes found within the lactate dehydrogenase promoter showed that mutations in either of the two E boxes severely affect Myc-dependent activation of transcription (T. Haggerty, and C.V. Dang, personal communication). These results suggest that Myc-Max complexes can form higher order structures that are consistent with the heterotetrameric assembly observed in our cocrystal structure.

An extensive network of hydrogen bonds and salt bridges mediates the protein-protein interface stabilizing the Myc-Max heterotetramer. Residues comprising this polar interaction network are unique to the Myc-Max heterodimer. Interestingly, the polarity of many of the residues in Myc that comprise the interaction network in the Myc-Max heterotetramer is altered in Mad. For example, Myc residue Glu425 is Arg127 in Mad, Arg423 of Myc is Glu125 in Mad, and His429 of Myc is Arg131 in Mad. Conceivably, this alteration in polarity of the residues that stabilize the interaction of the Myc-Max heterotetramer may explain the lack of tetramer formation by Mad-Max heterodimers in solution and in our cocrystals. It is possible that assembly of Myc-Max into bivalent heterotetramers allows for cooperative regulation at promoters and enhancers containing multiple E boxes.

Comparison with Long-Range Interactions Observed in c-Myb-C/EBPβ Cocrystal Structure

The bivalent assembly of Myc-Max heterodimers observed in our cocrystal structure recapitulates many structural elements found in the c-Myb-C/EBPβ cocrystal structure (Tahirov et al., 2002). The DNA binding domains of c-Myb and C/EBPβ interact in a head on fashion allowing for cooperative interaction, despite the fact that the individual proteins bind to widely separated sites on natural promoters. Atomic force microscopic studies, utilizing a synthetic promoter containing cognate recognition sites separated by 82 nucleotides, documented that the observed long-range interaction is mediated by DNA looping. This assembly of individual proteins components in the c-Myb-C/EBPβ cocrystal structure is analogous to dimerization of Myc-Max heterodimers to form the bivalent heterotetramer observed in our cocrystal structure. The carboxy-terminal coiled-coil of the C/EBPβ leucine zipper interacts with two α helices within c-Myb to form a four-helix bundle similar to the four-helix bundle that stabilizes the Myc-Max heterotetramer. v-Myb, which differs from c-Myb in the interfacial α helices, does not form a productive complex with C/EBPβ. The C/EBP family of proteins has a leucine zipper that is extended by one heptad repeat that undergoes a coil-to-helix transition upon binding to c-Myb (Tahirov et al., 2002).

The carboxy-terminal regions of C/EBPβ chains A and B form a polar interaction network with the exposed α helices of c-Myb (α-1 and α-2). A network of directional polar interactions (salt bridges and hydrogen bonds), are observed in the interface between c-Myb and C/EBPβ, where they appear to specify this particular binary complex. A similar network of salt bridges and hydrogen bonds specify the formation of the Myc-Max bivalent tetramer (see previous section for details). The solvent-accessible surface area buried between C/EBPβ and c-Myb is 1438 Å and is comparable to the estimated 1375 Å buried upon formation of the bivalent Myc-Max tetramer. Interactions among transcriptional factors bound to widely separated sites may be a general mechanism for the assembly of large nuclear complexes such as enhanceosomes (Carey, 1998; Merika and Thanos, 2001).

Conclusion

The cocrystal structures of the Myc-Max and Mad-Max heterodimers recognizing their E box targets demon-

strate how bHLHZ heterodimers can mediate specific, high-affinity DNA binding. Our structures and complementary biochemical findings suggest that two residues located within the C-termini of the leucine zipper regions are largely responsible for bHLHZ domains heterodimerization by Myc and Mad with Max. The crystal structure of the Myc-Max complex explains why this heterodimer, and only this heterodimer, can form a bivalent heterotetramer. Tetramerization of Myc and Max is mediated by extensive protein-protein interactions between leucine zipper domains, and the resulting antiparallel four-helix bundle could provide a scaffold for recruitment of additional modulators of transcription. Finally, our structures also provide a starting point for further directed biochemical and genetic studies to elucidate the roles played by Myc-Max and Mad-Max in cell fate determination.

Experimental Procedures

Protein and DNA Preparation and Crystallization

DNA fragment encoding the minimal bHLHZ regions of human Myc (residues 353–434), Max (residues 22–103), and Mad (residues 55–136) were amplified from corresponding full-length cDNAs and subcloned into a T7 RNA polymerase-dependent expression vector, which also produces an N-terminal polyhistidine tag and a C-terminal Gly-Gly-Cys tripeptide. (All other Cys residues within the bHLHZ portions of these proteins were changed to Ser.) Both Myc and Mad were purified from inclusion bodies by nickel-ion affinity chromatography under denaturing conditions. Max was purified using standard chromatographic methods as previously described (Ferre-D'Amare et al., 1993).

The reactive sulfhydryl group in Max-Gly-Gly-Cys was derivatized with 2,2′-dipyridyl disulfide, yielding a Max-pyridylsulfenyl cysteine adduct (Baca et al., 1995). The reaction product was purified from unreacted starting material with a Vydac C4 semi-preparative HPLC column using an acetonitrile gradient. The purified adduct was lyophilized and stored under anaerobic conditions. Chemoselective ligation of the Myc-Max heterodimer was performed by mixing equimolar quantities of Max-(2-pyridylsulfenyl) dissolved in 6 M guanidine-HCl with Myc-Gly-Gly-Cys and stirred at 4°C. Thiolysis of the Max-(2-pyridylsulfenyl) and formation of the desired chemoselectively ligated Myc-Max heterodimer was monitored by reverse-phase HPLC using a Vydac analytical C8 column and ESI-MS. Typical reaction times for product formation were 6 hr, after which the desired heterodimer was purified from starting materials on a Vydac semi-preparative C4 column. Product-containing fractions were pooled, lyophilized, dissolved in 6 M guanidine-HCl, and stored under nitrogen gas. Oligonucleotides were purified by reverse phase and ion exchange chromatographies. Immediately prior to crystallization experiments, the purified heterodimer was refolded by serial dialysis and excess oligonucleotide was added to the refolded heterodimer. Reconstituted protein-DNA complexes were purified from nonspecific aggregates and excess oligonucleotides were eliminated by size exclusion chromatography.

Myc-Max/DNA cocrystals were obtained by hanging drop vapor diffusion against 3–7% PEG 4000, 30% methyl pentane diol, 1 mM cobalt hexamine chloride, 50 mM sodium cacodylate [pH 6.5] at 15°C, using a protein concentration of 10 mg/mL and a 1:1 heterodimer:DNA ratio. Triclinic crystals grew in space group P1 ($\underline{a}$ = 39.2 Å, $\underline{b}$ = 45.1 Å, $\underline{c}$ = 86.5 Å, α = 87.9°, β = 84.6°, γ = 71.5°) with two protein-ligand complexes/asymmetric unit and diffract to at least 1.8 Å resolution using synchrotron radiation. Crystals of heavy atom derivatives were prepared with the same methods using oligonucleotides in which 5-iodo-dUra had been substituted for Thy (Figure 1).

Mad-Max DNA cocrystals were obtained by hanging drop vapor diffusion against 20% methyl pentane diol, 5 mM magnesium chloride, 50 mM sodium cacodylate [pH 6.0] at 15°C, using a protein concentration of 10 mg/mL and a 1:1 heterodimer:DNA molar ratio. These crystals also grew in the triclinic space group P1 ($\underline{a}$ = 47.4 Å, $\underline{b}$ = 56.0 Å, $\underline{c}$ = 65.6 Å, α = 88.8°, β = 79.1°, γ = 67.1°). Anisotropic diffraction was observed to 1.9 Å resolution at best, and 2.2 Å resolution elsewhere in the diffraction pattern.

Data Collection, Structure Determination, and Refinement

Native and heavy atom derivative diffraction data were collected using various synchrotron beamlines under standard cryogenic conditions. Data were processed using DENZO and SCALEPACK (Otwinowski, 1997). Structure determination was carried out with a 95.2% complete, 3-fold redundant native data set, with an overall $R_{sym}(I)$ = 5.3% (20–2.3 Å resolution). Heavy atom derivative data were typically obtained at a maximum resolution limits between 2.8–2.5 Å. Experimental phases were estimated at 2.8 Å resolution using SHARP, giving an overall figure of merit of 0.54 for acentric reflections. The resulting map was of poor quality despite reasonable phasing statistics, presumably due to heavy atom sites common to different heavy atom derivatives. The |Fobserved|/α(SHARP) electron density map was improved with density modification/histogram matching and the resulting phases (15–3.5 Å resolution) were used for brute force phased/rotation translation search (B. Strokopytov and S. Almo, personal communication) with X-PLOR (Brünger, 1992).

A bHLHZ search model was generated from our structure of the Max homodimer, with one protomer converted to polyalanine and both loop regions deleted, plus a minimal duplex DNA fragment encompassing only the E box hexanucleotide. The initial phased/rotation translation search yielded two significant solutions arranged as stacked bHLHZ dimers, which proved to be the two copies of the Myc-Max heterodimer comprising the bivalent heterotetramer (Figure 3C). These two solutions were then used to define the operators for 2-fold noncrystallographic symmetry averaging and phase extension to 2.5 Å, which yielded significant improvements in the quality of the electron density map. Interpretable electron density corresponding to regions of the protein that were not present in the initial search model and the entire DNA were readily discernible in this stage in structure determination.

Structure refinement was carried out with a 95% complete, 4-fold redundant data set with an overall $R_{sym}(I)$ = 5.3% (20–1.8 Å resolution). Several rounds of iterative model building and refinement were performed using O (Jones et al., 1991) and CNS (Brünger et al., 1998). The final model consists of two heterodimer-DNA complexes and 581 water molecules, giving an R-factor of 21.9% with R-free = 26.3%, and rmsds for bond lengths and angles of 0.005 Å and 0.95°, respectively. The mean thermal factors are 30 Å^2 for Myc and Max, 29 Å^2 for DNA, and 26 Å^2 for solvent molecules. PROCHECK (Laskowski et al., 1993) revealed five ($<$ 1.6%) unfavorable (ϕ,ψ) combinations in the Myc-Max complex, with main chain and side chain structural parameters consistently above average (overall G value = 0.1).

Structure determination of the Mad-Max heterodimer was carried out with a 98.4% complete, 4-fold redundant native data set, with an overall $R_{sym}(I)$ = 5.2% (20–2.5 Å resolution). The structure was solved by molecular replacement (Navaza, 1994) utilizing the following search model: partially refined Myc-Max heterodimer (R-free = 34.7%) with one protomer converted to polyalanine and both loop regions deleted plus a duplex DNA fragment encompassing the E box and appropriate flanking nucleotides. Subsequent refinement was performed against a 2.0 Å data set using O (Jones et al., 1991) and CNS (Brünger et al., 1998). The final model consists of two heterodimer-DNA complexes and 251 water molecules, giving an R-factor of 26.4%, with R-free = 32.4%, and rmsds for bond lengths and angles of 0.006 Å and 0.94°, respectively. The mean thermal factors are 47 Å^2 for Mad and Max, 48 Å^2 for DNA, and 49 Å^2 for solvent molecules. PROCHECK (Laskowski et al., 1993) revealed two ($<$ 0.7%) unfavorable (ϕ,ψ) combinations in the Mad-Max complex, with main chain and side chain structural parameters consistently above average (overall G value = 0.1).

The free R-value for this structure is somewhat higher than desirable, which may reflect the high level of disorder in the crystals as reflected by the high mean thermal factor values and such high free R-values have been reported for anisotropic data of similar resolution (Sui et al., 2001). We are, however, entirely confident of the validity of our Mad-Max cocrystal structure, which closely

resembles the structures of all extant bHLHZ proteins (Ferre-D'Amare et al., 1993; Parraga et al., 1998). Examination of difference electron density maps showed that modeling of solvent features was essentially complete and stereochemical parameters for the model are excellent.

Protein-Protein Interactions

A fragment of the gene encoding human Myc (corresponding to residues 353–434) was subcloned into pGEX-6P1 (Amersham Pharmacia). A glutathione S-transferase (GST)-Myc fusion and GST alone were expressed in *E. coli*, purified by glutathione-Sepharose chromatography, and dialyzed against binding buffer (100 mM NaCl, 20 mM HEPES [pH 7.5], 1 mM DTT, and 0.1% Triton X-100). Untagged Max (residues 22–103) was prepared and purified as described (Ferre-D'Amare et al., 1993). Mutants of Myc (Arg423→Gln; Arg424→Asn; Arg423→Gln/Arg424→Asn) and Max (Gln91→Arg; Gln92→Arg; Gln91→Arg/Asn92→Arg) were generated by the polymerase chain reaction using overlapping primers. GST (30 μg), GST-Myc (30 μg), and various GST-Myc mutants (30 μg) were each immobilized on 50 μl of glutathione-Sepharose resin (Amersham Pharmacia), and unbound protein was removed by washing. Ten μg of wild-type or mutant Max were added to 30 μl of either GST-resin or GST-Myc-resin. Binding reactions were diluted with 100 μl of binding buffer and incubated at 22°C for 30 min. After thrice washing with 100 μl of binding buffer, resin was harvested by centrifugation and bound proteins were visualized by gel electrophoresis.

Analytical Ultracentrifugation Studies

Sedimentation equilibrium data were collected at 280 nm with a rotor speed of 20,000 rpm at a temperature of 20°C in buffer solutions of 100 mM KCl, and 20 mM HEPES-KOH [pH = 7.5] using a Beckman XL-A ultracentrifuge. Solutions of the Myc-Max heterodimer were analyzed at three different concentrations of 0.252, 0.126, and 0.063 mM (corresponding to 5.34, 2.67, and 1.34 mg/ml, respectively). An extinction coefficient of 3960 A M^{-1} cm^{-1} and a partial specific volume of 0.73 cm^3/g were calculated from the amino acid sequence of the covalently linked Myc-Max heterodimer. Data analysis utilized the NONLIN program (http://www.cauma.uthscsa.edu/software).

Size Exclusion Chromatography

Approximately, 300 μM of the heterodimer was loaded onto a Superdex 75 (16/60) column (Pharmacia) and representative fractions from the elution run are shown on a Coomassie blue-stained SDS/PAGE gel. Elution volumes for four calibration standards are noted on the chromatogram.

Acknowledgments

At the National Synchrotron Light Source, we thank Drs. K.R. Rajashankar and Z.B. Dauter for support at Beamline X9B, and Dr. H. Lewis for support at Beamline X25; and at Argonne National Laboratories, we thank Drs. A. Joachimiak, S.L. Ginell, and F.J. Rotella for support at Beamline ID19. We thank Dr. J.B. Bonanno for assistance with data collection and Carme Edo and Hua Chen for technical help. We are grateful to Drs. R.N. Eisenman, D. Ayer, E. Ziff, T. Halazonetis, A. Ferre-D'Amare, A. Parraga, and C. Dang for providing cDNA clones and for insightful comments on Myc biology and bHLHZ structures. We also thank Drs. E.A. Campbell, S.A. Darst, R.C. Deo, K.S. Gajiwala, M. Huse, J. Kuriyan, T. Muir, and M. Young for many useful discussions. S.K.B. is an Investigator in the Howard Hughes Medical Institute. This work was supported by a grant from the N.I.H. S.K.N. was supported by a Leukemia Society of America postdoctoral fellowship and the Howard Hughes Medical Institute.

Received: June 28, 2002
Revised: December 13, 2002

References

Ayer, D.E., Kretzner, L., and Eisenman, R.N. (1993). Mad: a heterodimeric partner for max that antagonizes Myc transcriptional activity. Cell *72*, 211–222.

Ayer, D.E., Lawrence, Q.A., and Eisenman, R.N. (1995). Mad-Max transcriptional repression is mediated by ternary complex formation with mammalian homologs of yeast repressor Sin3. Cell *80*, 767–776.

Baca, M., Muir, T.W., Schnölzer, M., and Kent, S.B.H. (1995). Chemical ligation of cysteine-containing peptides: synthesis of a 22 kDA tethered dimer of HIV-1 protease. J. Am. Chem. Soc. *117*, 1881–1887.

Bao, J., and Zervos, A.S. (1996). Isolation and characterization of Nmi, a novel partner of Myc proteins. Oncogene *12*, 2171–2176.

Benvenisty, N., Ornitz, D.M., Bennett, G.L., Sahagan, B.G., Kuo, A., Cardiff, R.D., and Leder, P. (1992). Brain tumours and lymphomas in transgenic mice that carry HTLV-I LTR/c-myc and Ig/tax genes. Oncogene *7*, 2399–2405.

Blackwood, E., and Eisenman, R.N. (1991). Max: a helix-loop-helix zipper protein that forms a sequence-specific DNA-binding complex with Myc. Science *251*, 1211–1217.

Brownlie, P., Ceska, T., Lamers, M., Romier, C., Stier, G., Teo, H., and Suck, D. (1997). The crystal structure of an intact human Max-DNA complex: new insights into mechanisms of transcriptional control. Structure *5*, 509–520.

Brünger, A.T. (1992). X-PLOR: A system for X-ray crystallography and NMR. (New Haven: Yale University Press).

Brünger, A., Adams, P.D., Clore, G.M., Gros, P., Grosse-Kuntsleve, R.W., Jiang, J.-S., Kuszewski, J., Nilges, M., Pannu, N.S., and Read, R.J. (1998). Crystallography and NMR system: a new software system for macromolecular structure determination. Acta Crystallogr. D *54*, 905–921.

Carey, M. (1998). The enhanceosome and transcriptional synergy. Cell *92*, 5–8.

Coller, H.A., Grandori, C., Tamayo, P., Colbert, T., Lander, E.S., Eisenman, R.N., and Golub, T.R. (2000). Expression analysis with oligonucleotide microarrays reveals that MYC regulates genes involved in growth, cell cycle, signaling, and adhesion. Proc. Natl. Acad. Sci. USA *97*, 3260–3265.

Cole, M.D., and McMahon, S.B. (1999). The Myc oncoprotein: a critical evaluation of transactivation and target gene regulation. Oncogene *18*, 2916–2924.

Dalla-Favera, R., Bregni, M., Erikson, J., Patterson, D., Gallo, R.C., and Croce, C.M. (1982). Human c-myc onc gene is located on the region of chromosome 8 that is translocated in Burkitt lymphoma cells. Proc. Natl. Acad. Sci. USA *79*, 7824–7827.

Dang, C.V., Dolde, C., Gillison, M.L., and Kato, G.J. (1992). Discrimination between related DNA sites by a single amino-acid residue of Myc-related basic-helix-loop-helix proteins. Proc. Natl. Acad. Sci. USA *89*, 599–602.

Dang, C.V., McGuire, M., Buckmire, M., and Lee, W.M. (1989). Involvement of the 'leucine zipper' region in the oligomerization and transforming activity of human c-myc protein. Nature *337*, 664–666.

Dang, C.V., Resar, L.M., Emison, E., Kim, S., Li, Q., Prescott, J.E., Wonsey, D., and Zeller, K. (1999). Function of the c-Myc oncogenic transcription factor. Exp. Cell Res. *253*, 63–77.

Eilers, M. (1999). Control of cell proliferation by Myc family genes. Mol. Cells *9*, 1–6.

Eilers, M., Schirm, S., and Bishop, J.M. (1991). The MYC protein activates transcription of the alpha-prothymosin gene. EMBO J. *10*, 133–141.

Ellenberger, T.E., Brandl, C.J., Struhl, K., and Harrison, S.C. (1992). The GCN4 basic region leucine zipper binds DNA as a dimer of uninterrupted α helices: crystal structure of the protein-DNA complex. Cell *71*, 1223–1237.

Ferre-D'Amare, A.R., Prendergast, G.C., Ziff, E.B., and Burley, S.K. (1993). Recognition by Max of its cognate DNA through a dimeric b/HLH/Z domain. Nature *363*, 38–45.

Fisher, D.E., Parent, L.A., and Sharp, P.A. (1992). Myc/Max and other helix-loop-helix/leucine zipper proteins bend DNA toward the minor groove. Proc. Natl. Acad. Sci. USA *89*, 11779–11783.

Gaubatz, S., Imhof, A., Dosch, R., Werner, O., Mitchell, P., Buettner, R., and Eilers, M. (1995). Transcriptional activation by Myc is under negative control by the transcription factor AP-2. EMBO J. *14*, 1508–1519.

Grandori, C., and Eisenman, R.N. (1997). Myc target genes. Trends Biochem. Sci. *22*, 177–181.

Grandori, C., Mac, J., Siebelt, F., Ayer, D.E., and Eisenman, R.N. (1996). Myc-Max heterodimers activate a DEAD box gene and interact with multiple E box-related sites in vivo. EMBO J. *15*, 4344–4357.

Hassig, C.A., Fleischer, T.C., Billin, A.N., Schreiber, S.L., and Ayer, D.E. (1997). Histone deacetylase activity is required for full transcriptional repression by mSin3A. Cell *89*, 341–347.

Hill, C.P., Osslund, T.D., and Eisenberg, D. (1993). The structure of granulocyte-colony-stimulating factor and its relationship to other growth factors. Proc. Natl. Acad. Sci. USA *90*, 5167–5171.

Hurlin, P.J., Ayer, D.E., Grandori, C., and Eisenman, R.N. (1994). The Max transcription factor network: involvement of Mad in differentiation and an approach to identification of target genes. Cold Spring Harb. Symp. Quant. Biol. *59*, 109–116.

Janin, J. (1997). Specific versus non-specific contacts in protein crystals. Nat. Struct. Biol. *4*, 973–974.

Jones, T.A., Zou, J.Y., Cowan, S.W., and Kjeldgaard, M. (1991). Improved methods for building protein models in electron density maps and the location of errors in these models. Acta Crystallogr. A *47*, 110–119.

Kohl, N.E., Kanda, N., Schreck, R.R., Bruns, G., Latt, S.A., Gilbert, F., and Alt, F.W. (1983). Transposition and amplification of oncogene-related sequences in human neuroblastomas. Cell *35*, 359–367.

Kraulis, P.J. (1991). MOLSCRIPT: a program to produce both detailed and schematic plots of protein structures. J. Appl. Crystallogr. *24*, 946–950.

Kretzner, L., Blackwood, E.M., and Eisenman, R.N. (1992). Transcriptional activities of the Myc and Max proteins in mammalian cells. Curr. Top. Microbiol. Immunol. *182*, 435–443.

Laherty, C.D., Yang, W.M., Sun, J.M., Davie, J.R., Seto, E., and Eisenman, R.N. (1997). Histone deacetylases associated with the mSin3 corepressor mediate mad transcriptional repression. Cell *89*, 349–356.

Larsson, L.G., Bahram, F., Burkhardt, H., and Luscher, B. (1997). Analysis of the DNA-binding activities of Myc/Max/Mad network complexes during induced differentiation of U-937 monoblasts and F9 teratocarcinoma cells. Oncogene *15*, 737–748.

Larsson, L.G., Pettersson, M., Oberg, F., Nilsson, K., and Luscher, B. (1994). Expression of mad, mxi1, max and c-myc during induced differentiation of hematopoietic cells: opposite regulation of Mad and c-Myc. Oncogene *9*, 1247–1252.

Laskowski, R.A., MacArthur, M.W., Moss, D.S., and Thornton, J.M. (1993). PROCHECK: a program to check the stereochemical quality of protein structures. J. Appl. Crystallogr. *26*, 283–291.

Liao, D.J., and Dickson, R.B. (2000). c-Myc in breast cancer. Endocr. Relat. Cancer *7*, 143–164.

McArthur, G.A., Laherty, C.D., Queva, C., Hurlin, P.J., Loo, L., James, L., Grandori, C., Gallant, P., Shiio, Y., Hokanson, W.C., et al. (1998). The Mad protein family links transcriptional repression to cell differentiation. Cold Spring Harb. Symp. Quant. Biol. *63*, 423–433.

McMahon, S.B., Wood, M.A., and Cole, M.D. (2000). The essential cofactor TRRAP recruits the histone acetyltransferase hGCN5 to c-Myc. Mol. Cell. Biol. *20*, 556–562.

Merika, M., and Thanos, D. (2001). Enhanceosomes. Curr. Opin. Genet. Dev. *11*, 205–208.

Merritt, E.A., and Murphy, M.E.P. (1994). Raster3D Version 2.0, a program for photorealistic molecular graphics. Acta Crystallogr. D *50*, 869–873.

Moore, J.P., Hancock, D.C., Littlewood, T.D., and Evan, G.I. (1987). A sensitive and quantitative enzyme-linked immunosorbence assay for the c-Myc and n-myc oncoproteins. Oncogene Res. *2*, 65–80.

Nau, M.M., Brooks, B.J., Battey, J., Sausville, E., Gazdar, A.F., Kirsch, I.R., McBride, O.W., Bertness, V., Hollis, G.F., and Minna, J.D. (1985). L-Myc, a new Myc-related gene amplified and expressed in human small cell lung cancer. Nature *318*, 69–73.

Navaza, J. (1994). AmoRe: an automated program for molecular replacement. Acta Crystallogr. A *50*, 157–163.

Nekludova, L., and Pabo, C.O. (1994). Distinctive DNA conformations with enlarged major groove is found in Zn-finger-DNA and other protein-DNA complexes. Proc. Natl. Acad. Sci. USA *91*, 6948–6952.

Nesbit, C.E., Tersak, J.M., and Prochownik, E.V. (1999). MYC oncogenes and human neoplastic disease. Oncogene *18*, 3004–3016.

Nicholls, A., Sharp, K., and Honig, B. (1991). Protein folding and association: insights from the interfacial and thermodynamic properties of hydrocarbons. Proteins *11*, 281–296.

O'Hagan, R.C., Schreiber-Agus, N., Chen, K., David, G., Engelman, J.A., Schwab, R., Alland, L., Thomson, C., Ronning, D.R., Sacchettini, J.C., et al. (2000). Gene-target recognition among members of the myc superfamily and implications for oncogenesis. Nat. Genet. *24*, 113–119.

O'Shea, E.K., Klemm, J.D., Kim, P.S., and Alber, T. (1991). X-ray structure of the GCN4 leucine zipper, a two-stranded, parallel coiled coil. Science *254*, 539–544.

Otwinkowski, Z., and Minor, W. (1997). Processing of X-ray diffraction data collected in oscillation mode. In Meth. Enzymol., J. Charles, W. Carter, and R. M. Sweet, eds., pp. 307-326.

Parraga, A., Bellsolell, L., Ferre-D'Amare, A.R., and Burley, S.K. (1998). Co-crystal structure of sterol regulatory element binding protein 1a at 2.3Å resolution. Structure *6*, 661–672.

Peukert, K., Staller, P., Schneider, A., Carmichael, G., Hanel, F., and Eilers, M. (1997). An alternative pathway for gene regulation by Myc. EMBO J. *16*, 5672–5686.

Prendergast, G.C., Lawe, D., and Ziff, E.B. (1991). Association of Myn, the murine homolog of Max with c-Myc stiumulates methylation-sensitive DNA binding and Ras cotransformation. Cell *65*, 395–407.

Robinson, R.C., Grey, L.M., Staunton, D., Vankelecom, H., Vernallis, A.B., Moreau, J.F., Stuart, D.I., Heath, J.K., and Jones, E.Y. (1994). The crystal structure and biological function of leukemia inhibitory factor: implications for receptor binding. Cell *77*, 1101–1116.

Rudolph, C., Adam, G., and Simm, A. (1999). Determination of copy number of c-Myc protein per cell by quantitative Western blotting. Anal. Biochem. *269*, 66–71.

Sakamuro, D., and Prendergast, G.C. (1999). New Myc-interacting proteins: a second Myc network emerges. Oncogene *18*, 2942–2954.

Saleh, A., Schieltz, D., Ting, N., McMahon, S.B., Litchfield, D.W., Yates, J.R., Lees-Miller, S.P., Cole, M.D., and Brandl, C.J. (1998). Tra1p is a component of the yeast Ada.Spt transcriptional regulatory complexes. J. Biol. Chem. *273*, 26559–26565.

Schreiber-Agus, N., Chin, L., Chen, K., Torres, R., Rao, G., Guida, P., Skoultchi, A.I., and DePinho, R.A. (1995). An amino-terminal domain of Mxi1 mediates anti-Myc oncogenic activity and interacts with a homolog of the yeast transcriptional repressor SIN3. Cell *80*, 777–786.

Schwab, M., Varmus, H.E., Bishop, J.M., Grzeschik, K.H., Naylor, S.L., Sakaguchi, A.Y., Brodeur, G., and Trent, J. (1984). Chromosome localization in normal human cells and neuroblastomas of a gene related to c-Myc. Nature *308*, 288–291.

Sheiness, D., Fanshier, L., and Bishop, J.M. (1978). Identification of nucleotide sequences which may encode the oncogenic capacity of avian retrovirus MC29. J. Virol. *28*, 600–610.

Shim, H., Dolde, C., Lewis, B.C., Wu, C.S., Dang, G., Jungmann, R.A., Dalla-Favera, R., and Dang, C.V. (1997). c-Myc transactivation of LDH-A: implications for tumor metabolism and growth. Proc. Natl. Acad. Sci. USA *94*, 6658–6663.

Somers, W., Stahl, M., and Seehra, J.S. (1997). 1.9 Å crystal structure of interleukin 6: implications for a novel mode of receptor dimerization and signaling. EMBO J. *16*, 989–997.

Sui, H., Han, B.G., Lee, J.K., Walian, P., and Jap, B.K. (2001). Structural basis of water-specific transport through the AQP1 water channel. Nature *414*, 872–878.

Taub, R., Kirsch, I., Morton, C., Lenoir, G., Swan, D., Tronick, S., Aaronson, S., and Leder, P. (1982). Translocation of the c-myc gene into the immunoglobulin heavy chain locus in human Burkitt lymphoma and murine plasmacytoma cells. Proc. Natl. Acad. Sci. USA *79*, 7837–7841.

Tahirov, T.H., Sato, K., Ichikawa-Iwata, E., Sasaki, M., Inoue-Bungo, T., Shiina, M., Kimura, K., Takata, S., Fujikawa, A., Morii, H., et al. (2002). Mechanism of c-Myb-C/EBPβ cooperation from separated sites on a promoter. Cell *108*, 57–70.

Wang, Q., Zhang, H., Kajino, K., and Greene, M.I. (1998). BRCA1 binds c-Myc and inhibits its transcriptional and transforming activity in cells. Oncogene *17*, 1939–1948.

Watson, D.K., Psallidopoulos, M.C., Samuel, K.P., Dalla-Favera, R., and Papas, T.S. (1983). Nucleotide sequence analysis of human c-Myc locus, chicken homologue, and myelocytomatosis virus MC29 transforming gene reveals a highly conserved gene product. Proc. Natl. Acad. Sci. USA *80*, 3642–3645.

Watt, R., Stanton, L.W., Marcu, K.B., Gallo, R.C., Croce, C.M., and Rovera, G. (1983). Nucleotide sequence of cloned cDNA of human c-Myc oncogene. Nature *303*, 725–728.

Winston, R.L., and Gottesfeld, J.M. (2000). Rapid identification of key amino-acid-DNA contacts through combinatorial peptide synthesis. Chem. Biol. *7*, 245–251.

Zervos, A.S., Gyuris, J., and Brent, R. (1993). Mxi1, a protein that specifically interacts with max to bind Myc-Max recognition sites. Cell *72*, 223–232.

Accession Numbers

The Protein Data Bank accession number for the Myc-Max cocrystal structure is 1NKP and for the Mad-Max concrystal structure is 1NLW.